Available online at www.sciencedirect.com
ScienceDirect
Metabolism Clinical and Experimental 59 (2010) 1124 – 1138
Metabolism
Clinical and Experimental
www.metabolismjournal.com

Metabolic signs of vitamin B_{12} deficiency in humans: computational model and its implications for diagnostics

Sergey N. Fedosov*

Protein Chemistry Laboratory, Department of Molecular Biology, University of Aarhus, Science Park, DK 8000 Aarhus C, Denmark

Received 12 November 2008; accepted 17 September 2009

Abstract

Early diagnostics of cobalamin (Cbl, vitamin B_{12}) deficiency is primarily based on measurements of the relevant metabolic markers in blood plasma—total B_{12}, specific Cbl-saturated transporter holo-transcobalamin (holoTC), and substrates of Cbl-dependent enzymatic reactions methylmalonic acid (MMA) and homocysteine (Hcy). Concentrations of B_{12} and holoTC decrease whereas MMA and Hcy increase under deficiency. Yet, the results of individual tests are often contradictory and do not guarantee unambiguous diagnosis. The current work describes the metabolic manifestation of vitamin B_{12} deficiency in terms of flux equations fitted to data sets from literature. The model mathematically connects all the markers and presents 4 independent measurements as a single point (x, y) in the combined coordinates $x = (\text{holoTC}\cdot B_{12})^{1/2}$ and $y = \frac{1}{2}\log_{10}(\text{MMA}\cdot\text{Hcy})$. Pairwise averaging compensates for the individual fluctuations of the markers caused by (1) irregular spikes of holoTC, (2) delayed change of the total plasma B_{12} buffered by an internal Cbl depot, and (3) variations in the production/excretion velocities of MMA and Hcy. Bivariate distribution of the marker combinations (x, y) reveals several peaks of frequency in the analyzed mixed population. The peaks seem to represent the reference subgroups with different B_{12} physiology and characteristic values of "wellness parameter": $w = \log_{10}(\text{holoTC}_n) + \log_{10}(B_{12n}) - \log_{10}(\text{MMA}_n) - \log_{10}(\text{Hcy}_n)$, where concentrations are normalized (eg, $\text{MMA}_n = \text{MMA}/\text{MMA}_{\text{normal}}$). Dynamic response of the organism to B_{12} intake is quantified and described as an additional analytical tool when classifying uncertain cases. The discussed mathematical approaches are of general applicability in diagnostics.

1. Introduction

Vitamin B_{12}, or cobalamin (Cbl), is an important cofactor in human metabolism. Its uptake from dietary sources (meet, milk, etc) requires an intricate transportation mechanism, which involves several specific protein carriers and receptors [1-4]. Two major transporters of B_{12} in blood are transcobalamin (TC) and haptocorrin (HC) [1,2,4]. Transcobalamin is involved in distribution of B_{12} between different tissues, and the level of holo-transcobalamin (holoTC; TC·Cbl complex) increases after intake of a new portion of the vitamin [5]. Later on, a part of the assimilated Cbl reappears in blood bound to the second carrier HC [1]. The function of the latter is not completely elucidated, but storage of B_{12} and scavenging of B_{12} analogues are often mentioned in this context [1,2,4].

Hereditary or acquired damage of the transportation chain causes gradual Cbl depletion. Among the consequences of B_{12} deficiency are (1) hampered conversion of methylmalonic acid (MMA) to succinate [6] and (2) deactivation of folate by "methyltetrahydrofolate trap" [7]. The earliest symptoms of B_{12} insufficiency include accumulation of MMA and homocysteine (Hcy) in blood contributing to vascular pathogenesis. The later stages of the disease reveal different neurologic disorders and/or anemia [7-10]. Without treatment, the outcome is lethal.

The B_{12} deficiency becomes a growing public health problem in parallel with the increase of elderly population, where approximately 15% suffer from mild to severe symptoms of the disease [8]. Because the evident signs of B_{12} deficiency appear relatively late and are often accompanied by irreversible damage to the nervous system, the metabolic detection of the disease at an early subclinical stage is of primary importance [8,9].

The laboratory evaluation of B_{12} status follows different strategies whose advantages and disadvantages are intensely

* Tel.: +45 89 42 50 90; fax: +45 86 13 65 97.
E-mail address: snf@mb.au.dk.

0026-0495/$ – see front matter © 2010 Elsevier Inc. All rights reserved.
doi:10.1016/j.metabol.2009.09.036

debated [8,9,11-17]. Measurement of the total B_{12} in blood plasma (Cbl-saturated HC [holoHC] + holoTC) has been used for decades because of the simplicity of the method. At the same time, the level of total B_{12} poorly correlates with other indications of the vitamin insufficiency [8,9,11-17]. Another approach is based on measurement of B_{12}-related metabolites, MMA and total Hcy, usually increased under Cbl insufficiency [6,7,9]. Yet, the abnormal levels of MMA and Hcy are often not related to low B_{12} (see for example reviews by Baik and Russell [8] and by Carmen et al [9]).

It has also been hypothesized that the Cbl-saturated transporting protein holoTC (present in plasma) is a better indicator of the true B_{12} status when compared with the 3 previously mentioned markers [18]. Therefore, the recent appearance of a sensitive test on serum holoTC in several modifications [19-21] was followed by intensive examinations of holoTC levels in different groups of patients. Some authors found a better predictability of B_{12} status using holoTC test [13,17,20,22], whereas others disclaimed superiority of holoTC analysis [15,16,22].

Application of biochemical markers for an early detection of B_{12} deficiency is becoming widespread [6,8,9,11-17,20,22] because clinical indications are inconclusive unless the disease becomes life-threatening [9]. For example, absence of correlation between the clinical and metabolic signs was established for patients in the transitional phase [9,12,22]. Presently, there is no clearly superior strategy of an early detection of Cbl deficiency. All biochemical markers (total plasma B_{12}, holoTC, MMA, and Hcy) are often measured to examine the Cbl-related metabolism in general terms. This "extensive" approach is now routinely used in many clinical laboratories [11-17,20,22]. At the same time, interpretation of the obtained results presents some difficulties. By common assent, identification of the high risk group is based on the approximate threshold limits, for example, holoTC, less than 35 pmol/L; B_{12}, less than 150 pmol/L; MMA, greater than 0.5 μmol/L; and Hcy, greater than 15 μmol/L. Yet, indications from 4 independent tests frequently contradict each other, compromising accuracy of diagnostics in the absence of one criterion standard (discussed by Carmel et al [9]).

The current publication attempts to improve diagnostics of B_{12} deficiency by connecting all metabolic indicators within a network of fluxes and analyzing them simultaneously. Effect of B_{12} on the steady-state concentrations of metabolites is simulated in different coordinate systems, and the curves agree with the experimental database. Best correlation is achieved using the averaging surface, which presents the data for each individual as a single point positioned with higher precision. The reduced dispersion facilitates statistical analysis, and the detected frequency peaks are suggested as the metabolic fingerprints of different (sub)clinical phenotypes. Ambiguous steady-state measurements are additionally examined for their dynamics because differentiation compensates the major error of steady-state analysis according to modeling. The produced reference tables and charts are expected to facilitate practical diagnostics based on metabolic measurements.

2. Methods

2.1. Glossary

Populations: Hlt—healthy, HltB—healthy treated with B_{12}, Sus—suspected of being B_{12} deficient, and *Veg*—vegans.

Subgroups with different B_{12} status: *e*—excellent, *n*—normal, *t*—transitional, *d*—deficient, and *p*—pernicious.

Parameters of a metabolic flux: v_i—velocity of a flux numbered as i, V_i—maximal v_i; K_i—half-saturation coefficient of a quasi-hyperbolic flux, k_i—slope coefficient of a quasi-linear flux, and S_i—substrate of flux v_i.

Metabolites in schemes: M_1—holoTC, M_2—holoHC, and S—MMA or Hcy.

Fitting parameters P_i: combinations of rate constant described in Eq. (9a, 9b, 9c).

Combined variables: $x = (\text{holoTC}\cdot B_{12})^{1/2}$; $y = \frac{1}{2}\log_{10}(\text{MMA}\cdot\text{Hcy})$; and $w = \log_{10}(\text{holoTC}_n) + \log_{10}(B_{12n}) - \log_{10}(\text{MMA}_n) - \log_{10}(\text{Hcy}_n)$, wellness parameter, where variables correspond to the normalized concentrations; for example, $\text{MMA}_n = \text{MMA}/\text{MMA}_{\text{normal}}$.

2.2. Analyzed data sets

The data sheets containing plasma concentrations of holoTC, total B_{12}, MMA, and total Hcy in healthy individuals and patients were kindly provided by the authors of the original publications [14,17,22]. The data included 3 populations, preselected according to the criteria below. None of the examined persons was clearly B_{12} deficient, yet some of them had metabolic or/and clinical signs of the vitamin deficiency.

The first group [14] represented apparently healthy volunteers. Measurements of 4 markers were undertaken at first visit (day 1) and after receiving several oral doses of B_{12} (3×9 μg/d for 5 days). The final measurements were performed at day 8. Two sets of data obtained from the same group at day 1 or day 8 were called population *Healthy* (Hlt) or population *Healthy + B_{12}* (HltB), respectively.

Another large group [22] included individuals suspected of being B_{12} deficient because of increased concentration of MMA (>0.28 μmol/M) measured in other context within 4 years before examination. A significant part of this group (61%) had at least one clinical sign potentially related to B_{12} deficiency at first visit [22]. Yet, none of the patients was clearly deficient and received B_{12} treatment. The authors also found no association of clinical symptoms and biochemical indications within this group called here *Suspected* (Sus).

The third population [17] represented generally healthy vegans who did not have a history of serious medical disorders. The concentrations of B_{12} expressed in nanograms per liter [17] were recalculated to picomoles per liter using coefficient ×1/1.35. This data set was called *Vegans* (Veg).

Further selection was performed before the current analysis. Thus, individuals (1) lacking measurements of one or more markers, (2) characterized by increased plasma creatinine (>100 μmol/L), or (3) with unreliable determination of either holoTC (<1 or >500 pmol/L) or B_{12} (>1000 pmol/L) were excluded. Finally, the following data sets were analyzed: Hlt (n = 74), Sus (n = 647), and Veg (n = 144).

Statistical analysis and fitting procedures were performed with help of a computer program KyPlot 5 (KyensLab Inc., Tokyo, Japan).

2.3. Methods of mathematical analysis

2.3.1. General principles of flux approximation

Measurement of a metabolic marker in blood reflects its current steady-state concentration. The latter is determined by velocities of ingoing and outgoing fluxes within a network of metabolic processes (examples in Fig. 1). One individual metabolic branch (flux v) may include either one reaction (eg, $S \rightarrow P$) or a sequence of reactions (eg, $S \rightarrow X_1 \rightarrow X_2 \ldots \rightarrow P$). Velocity of such process is often approximated by a quasi hyperbole, a line, or an empiric LinLog function $v = a' + b' \cdot \log(S)$ (see Legent et al [23] and Wu et al [24] for discussion). The current publication argues for the following flux equations:

$$v \approx \frac{V \cdot S}{K + S} \tag{1}$$

$$v \approx \frac{V}{1.5 \cdot K} \cdot S = k \cdot S \tag{2}$$

$$v \approx \frac{V}{2} \cdot \left\{ 1 + log_{10}\left(\frac{S}{K}\right) \right\} \tag{3}$$

where V is the maximal velocity of flux and K is the constant of half-response to S. Both V and K are combinations of different rate constants within the corresponding flux. The mathematical background of Eqs. (1), (2), and (3) is presented in "Appendix A" ("Mathematical justification of flux equations").

The equations are generic and applicable to any flux disregarding the number of elementary steps within it. The shape of the curve v vs S (hyperbolic, quasi-hyperbolic, linear, or logarithmic) depends on the combination of internal rate constants [23] and cannot be predicted without the intimate knowledge of each individual step. In the absence of such knowledge, a few trials are required to reach a fair correlation between the model and the experimental data. The approach to approximation of a data set is unique in each particular case, although there are a few guidelines. Thus, the hyperbolic function Eq. (1) is expected to give a relatively accurate approximation [23]; yet the mathematical solution of a system of hyperbolic equations can be very complex. Linear approximation Eq. (2) is convenient in terms of mathematics and is sometimes sufficiently accurate [23]; however, it would always give a noticeable deviation at saturating S. Logarithmic function Eq. (3) is sufficiently accurate and has simple mathematics, yet the flux velocity v becomes negative at low S (which restricts the diapason of application to $S/K > 0.1$).

2.3.2. Dependence of total plasma B_{12} on holoTC (scheme 1)

Initial trials indicated that an empiric fitting function constructed of hyperbolic and linear components Eq. (1) + Eq. (2) provided a better approximation ($R^2 = 0.47$) when compared with a hyperbole Eq. (1), $R^2 = 0.39$; a line Eq. (2), $R^2 = 0.11$; or a LinLog function Eq. (3), $R^2 = 0.39$. Several schemes might serve as a basis for the preferable fitting function.

The simplest model includes fluxes v_0, v_1, and v_2 (part of scheme 1 in Fig. 1) and follows the generally accepted route of Cbl circulation (see reviews by Allen [1], Fedosov [2], Moestrup and Verroust [3], and Nexø [4]). It comprises (1)

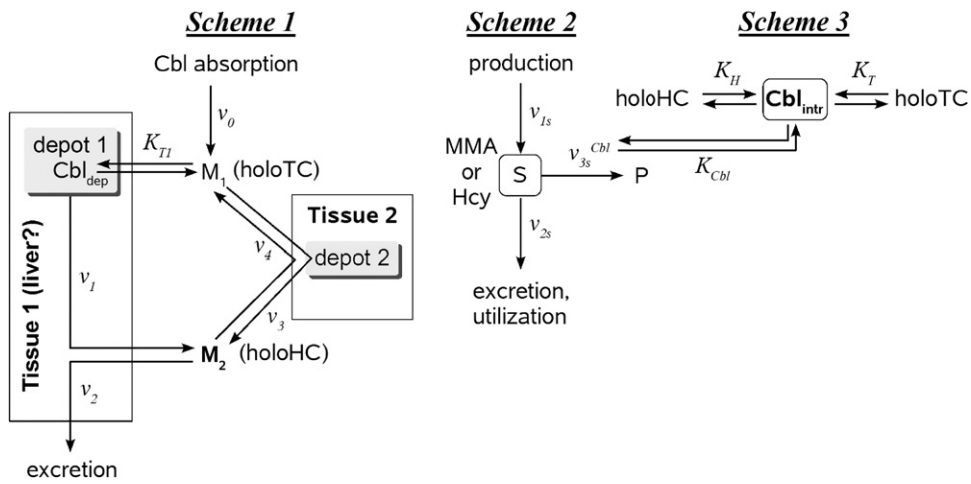

Fig. 1. Metabolic schemes: (1) transportation network of plasma Cbl; (2) turnover of MMA and Hcy in plasma; (3) equilibriums between the intracellular Cbl and the extracellular carriers of the vitamin. See "Methods" for the details.

first appearance of the absorbed vitamin in blood as holoTC (M_1), (2) exchange of Cbl between holoTC and the intracellular pool accompanied by accumulation of Cbl in some tissues (eg, liver) called *depot 1* (where $Cbl_{dep} = K_{T1} \cdot M_1$), (3) partial recirculation of Cbl_{dep} as holoHC (M_2), and (4) final excretion of holoHC to the digestive tract with bile. This straightforward model with fluxes v_0 (a constant), v_1 (a hyperbole), and v_2 (either a hyperbole or a line) was, however, unsatisfactory. It is easy to demonstrate that such kinetic scheme stipulates the slope of linear component equal to 1 (ie, $K_{34} = 0$; see Eq. [5] below), whereas the unconstrained fitting gave a value of 1.9 ± 0.2 (Fig. 2A).

This inconsistency was circumvented using a branched model (scheme 1 in Fig. 1) supplemented by 2 additional routes, v_3 and v_4. They describe exchange of Cbl between TC and HC via degradation of both proteins inside a tissue compartment called *depot 2*. The direct ligand exchange between TC and HC was not considered because affinities of both proteins for Cbl are too high ($K_d = 10^{-15}$ mol/L) to expect any dissociation in a real-time scale [25,26]. The final scheme included the following fluxes: v_0—a constant; v_1—approximated by Eq. (1), with parameters V_1 K_1; v_2, v_3, and v_4—approximated by Eq. (2) with parameters k_2, k_3, and k_4, respectively.

The steady-state balance of M_2 (holoHC) was described by the below equation:

$$\frac{dM_2}{dt} = v_1 + v_3 - v_2 - v_4 = 0 \tag{4}$$

After a few simple transformations, M_2 was expressed via M_1 (considering $Cbl_{dep} = K_{T1} \cdot M_1$); and the total plasma B_{12} was presented as $M_2 + M_1$:

$$B_{12} = \frac{V_{d1} \cdot M_1}{K_{d1} + M_1} + (1 + K_{34}) \cdot M_1 \tag{5}$$

where $V_{d1} = \frac{V_1}{k_4 + k_2}$; $K_{d1} = \frac{K_1}{K_{T1}}$; $K_{T1} = \frac{k_{+T1}}{k_{-T1}}$; $K_{34} = \frac{k_3}{k_4 + k_2}$

More detailed interpretation of the model and its coefficients is given in "Results" and "Discussion." Note that the assignment $k_2 = 0$ or $k_4 = 0$ makes no difference to the fitting behavior of Eq. (5).

2.3.3. Transitional effects in scheme 1

In a real situation, occasional unbalanced fluctuations of M_1 and M_2 are possible. The transitional (non–steady-state) kinetics would be revealed in coordinates total B_{12} vs M_1 (Fig. 2) as deviation of B_{12} from zero at $M_1 \rightarrow 0$. Therefore, expression Eq. (5), suitable only for a stationary case, was substituted by the equation with floating zero:

$$B_{12} = \frac{V_{d1} \cdot (M_1 + \delta M_1)}{K_{d1} + (M_1 + \delta M_1)} + (1 + K_{34}) \cdot M_1 \tag{6}$$

where δM_1 is proportional to the concentration of Cbl_{dep}, either absorbed by the depleted depot 1 without any leakage of holoHC ($\delta M_1 < 0$) or provided by the saturated depot 1 as a surplus flow of holoHC ($\delta M_1 > 0$). Detailed mechanisms of the above effects are not specified because of lack of information. Exchange of Cbl via depot 2 remains unaffected.

2.3.4. Dependence of MMA and Hcy on Cbl (scheme 2)

Turnover of a blood plasma metabolite *S* (substrate of Cbl-dependent reaction) is depicted in scheme 2 (Fig. 1). It considers presence of one influx, v_{1s} (production of *S*), and 2 effluxes, v_{2s} and v_{3s}. The influx v_{1s} corresponds to either synthesis of MMA in the course of degradation of fatty acids [6] or production of Hcy after methylations involving *S*-adenosylmethionine [7]. The first outgoing branch, v_{2s}, reflects excretion or/and enzymatic consumption of *S* with no relation to Cbl [6,7,27,28]. The second efflux, v_{3s}, represents the Cbl-dependent reaction (either methylmalonyl–coenzyme A mutase for MMA or methionine synthase for Hcy) [6,7]. Equilibriums in scheme 3 (Fig. 1) connect the extracellular and intracellular pools of Cbl, which makes scheme 3 a component of scheme 2. Tissue distribution of the 3 fluxes is not specified because the plasmatic and intracellular pools of *S* are connected via a single constant, K_{eq}. Introduction of the latter does not change the general appearance of the final fitting function (see the analogous issue in scheme 1).

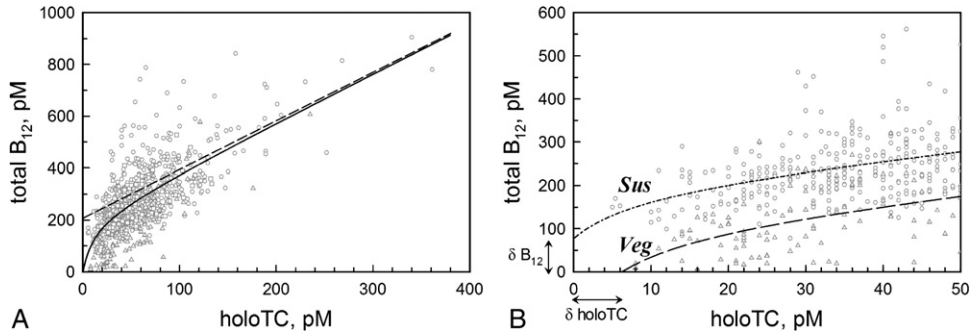

Fig. 2. Dependence of the total plasma B_{12} on holoTC in populations Hlt (□), Sus (○), and Veg (Δ). A, Full-scale coordinates. The best fit (Eq. [5]) and its linear component are indicated by solid and dashed lines, respectively. B, Low-concentration region. The fitting function with floating zero (Eq. [6]) was used to approximate populations Sus (dash-dotted line) and Veg (long dashes) taken separately.

The designed model aims to express S or $\log(S)$ as a function of Cbl using the steady-state balance below:

$$\frac{dS}{dt} = v_{1s} - v_{2s} - v_{3s} = 0 \tag{7}$$

Eq. (7) cannot be solved algebraically using exclusively hyperbolic approximations of v_i via Eq. (1). Combination of hyperbolic and linear functions was also abandoned because of an inadequate fitting of the experimental data in Fig. 3 (not shown). The satisfactory solution was, however, achieved using LinLog functions ("Extended solution of scheme 2" in "Appendix A"). The influx of S (v_{1s}) was set as a constant parameter because this assumption simplifies the solution but does not affect the appearance of final equation.

Expression of $\log_{10}(S)$ as a function of Cbl is derived in "Appendix A":

$$log_{10}(S) = P_{1s} - \frac{P_{2s} \cdot X}{P_{3s} + X} \tag{8}$$

Notation of variables is as follows: S = MMA or Hcy; X = holoTC, B_{12}, or $(B_{12}\cdot\text{holoTC})^{1/2}$. Parameters P_i are combinations of constants:

$$P_{1s} = \frac{2 \cdot v_{1s}}{V_{2s}} - 1 + log_{10}(K_2) \tag{9a}$$

$$P_{2s} = \{1 + P_{1s} - log_{10}(K_3)\} \cdot \frac{V_{3s}}{V_{2s} + V_{3s}} \tag{9b}$$

$$P_{3s} = \frac{V_{2s}}{V_{2s} + V_{3s}} \cdot K_X \tag{9c}$$

where v_{1s} is a constant; V_{2s}, V_{3s}, K_2, and K_3 are the maximal velocities and the corresponding half-saturation coefficients of the fluxes v_{2s} and v_{3s} (scheme 2); and $K_X = K_{Cbl}/K_B$, K_{Cbl}/K_T, and K_{Cbl}/K_{BT} are the ratios of equilibrium constants consistent with the chosen variable X = total B_{12}, holoTC, or $(B_{12}\cdot\text{holoTC})^{1/2}$, respectively. Note that P_is do not specify the ratios S/K_i, and the obligatory requirement of the LinLog kinetics (S/K_i >0.1) is never violated under the data fitting.

If the P_{3s} values in Eq. (8) for log(MMA) and log(Hcy) dependencies on X (Fig. 3A, B, C) turn out to be similar, the 2 functions can be averaged, maintaining the hyperbolic shape of the produced curve. Otherwise, the sum of 2 hyperboles multiplied by ½ is the correct answer. In the present case, equivalence of P_{3s} was very probable (45%-78% according to t test of the data in Table 1); and the single-hyperbole approximation was used:

$$y = P_1 - \frac{P_2 \cdot x}{P_3 + x} \tag{10}$$

where $y = ½\log_{10}(\text{MMA}\cdot\text{Hcy})$; $x = X$; $P_1 = ½(P_{1MMA} + P_{1Hcy})$; $P_2 = ½(P_{2MMA} + P_{2Hcy})$; and $P_3 \approx P_{3MMA} \approx P_{3Hcy}$.

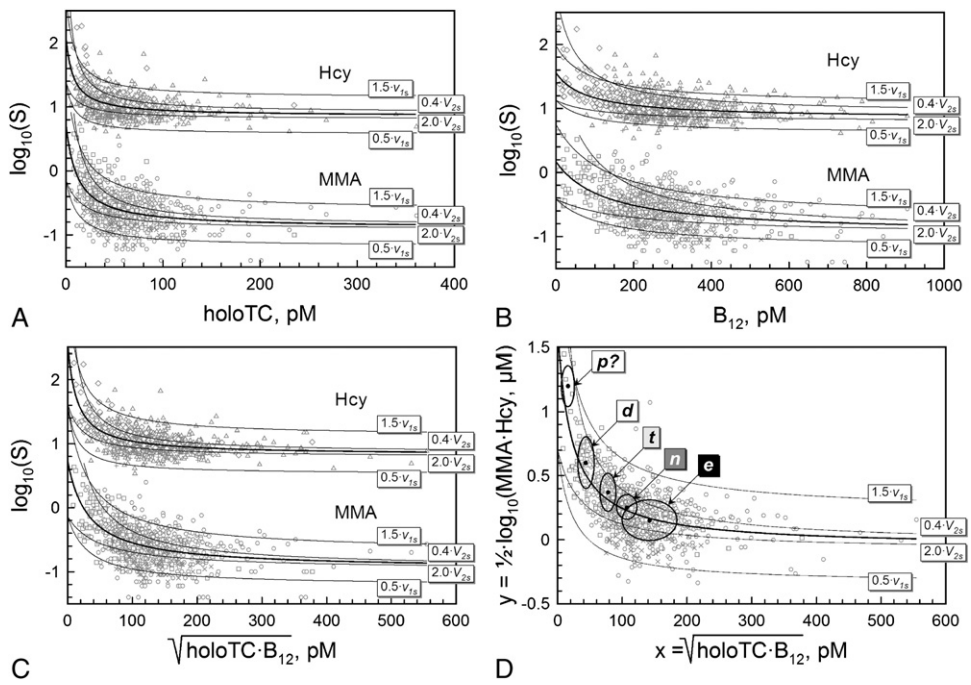

Fig. 3. Metabolites MMA (× ○□) and Hcy (+Δ◊) (in micromoles per liter) as logarithmic functions of (A) holoTC, (B) total B_{12}, and (C) $(\text{holoTC}\cdot B_{12})^{1/2}$ and (D) when plotted in the semilogarithmic geometric mean coordinates. The pooled data for populations Hlt (× +), Sus (○Δ), and Veg (□◊) were approximated by Eqs. (8) and (10). See the main text for details. The optimal fits are depicted by thick lines. Thin lines illustrate behavior of the system with altered v_{1s} and V_{2s}. See scheme 2. Ellipses in panel D include 68% of the subgroups p, d, t, n, and e (with assumed pernicious, deficient, transitional, normal, and excellent B_{12} status). Centers and radii of ellipses correspond to $\mu_{i,xy}$ and $\pm\,\sigma_{i,x} \pm \sigma_{i,y}$, respectively.

Table 1
Fitting parameters (mean ± SE) for MMA and Hcy dependencies on holoTC and B_{12} (Fig. 3)

Dependency	P_1	P_2	P_3 (pmol/L)	R^2
Fig. 3A log(MMA) vs holoTC	0.70 ± 0.32	1.6 ± 0.29	11.9 ± 4.4	0.18
Fig. 3A log(Hcy) vs holoTC	2.05 ± 0.30	1.19 ± 0.28	8.0 ± 3.2	0.10
Fig. 3B log(MMA) vs B_{12}	0.17 ± 0.50	1.12 ± 0.40	130 ± 130	0.091
Fig. 3B log(Hcy) vs B_{12}	1.55 ± 0.53	0.71 ± 0.48	82 ± 109	0.071
Fig. 3C log(MMA) vs $(holoTC \cdot B_{12})^{1/2}$	0.72 ± 0.60	1.67 ± 0.54	32 ± 20	0.18
Fig. 3C log(Hcy) vs $(holoTC \cdot B_{12})^{1/2}$	2.55 ± 1.17	1.73 ± 1.14	14.1 ± 13.0	0.13
Fig. 3D ½log(MMA·Hcy) vs $(holoTC \cdot B_{12})^{1/2}$	1.56 ± 0.20	1.62 ± 0.18	23.0 ± 5.3	0.41

The dependence starts at the point with coordinates $x = 0$, $y = P_1$ and tends to $x \to \infty$, $y \to (P_1 - P_2)$ with the half effect at $x = P_3$ (Fig. 3).

Application of the combined coordinates x, y for the data fitting reduces both horizontal (x) and vertical (y) dispersion because each experimental point originates, in fact, from 4 measurements instead of 2.

2.3.5. Statistical analysis of distributions

Probability distribution of a variable (x) is often presented as a frequency polygon to detect skewed or polymodal shape. The frequency distributions of B_{12} markers (Fig. 4) were examined in this way for presence of multiple subgroups. The charts were fitted by a sum of Gaussian functions [29-31]:

$$f_{(x)} = \sum F_i \cdot e^{-\frac{(x-\mu_i)^2}{2\sigma_i^2}} \quad (11)$$

where $f_{(x)}$ is the frequency of measurements registered at x; F_i is the local frequency peak; μ_i represents the x coordinate of F_i peak (the mean of a subgroup); and σ_i is its standard deviation.

Simultaneous analysis of 4 metabolic markers of B_{12} deficiency necessitates application of multivariate statistics. A bivariate case was considered where distribution of points with coordinates $x = (holoTC \cdot B_{12})^{1/2}$ and $y = ½\log_{10}$

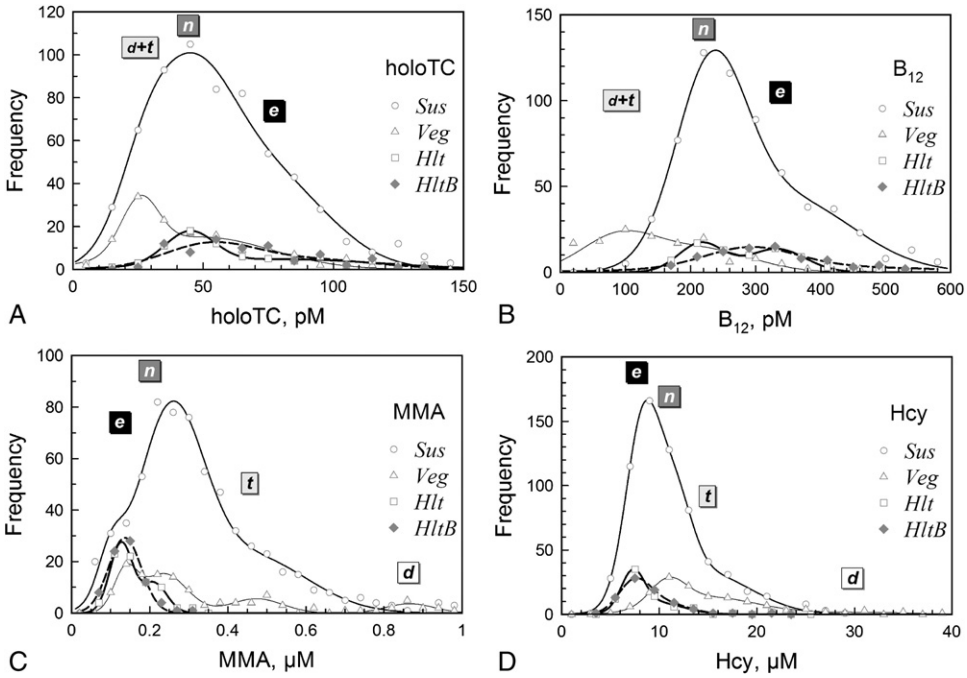

Fig. 4. Frequency distributions of (A) holoTC, (B) total B_{12}, (C) MMA, and (D) Hcy in the populations Hlt (thick line), HltB (thick dashed line), Sus (intermediate line), and Veg (thin line). Approximate positions of the *e*, *n*, *t*, and *d* peaks (excellent, normal, transitional, and deficient B_{12}) are marked with tags.

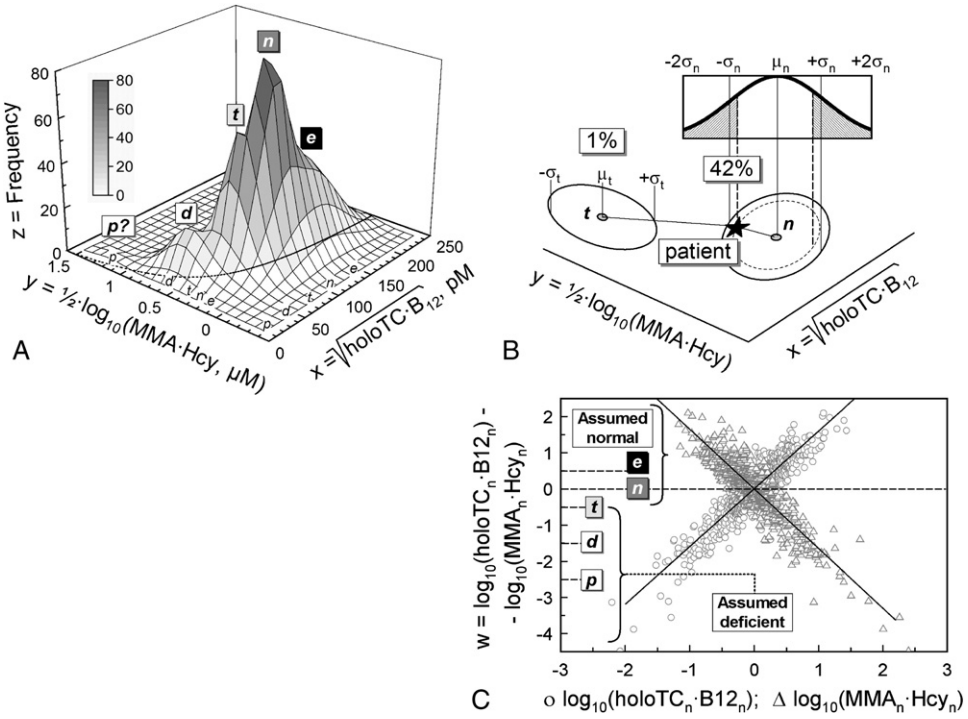

Fig. 5. Combined variables in evaluation of B_{12} status. A, Bivariate frequency distribution of the combined variables x, y. Maximums of the subgroups are marked with tags *e*, *n*, *t*, *d*, and *p* (excellent, normal, transitional, deficient, and pernicious types). The fit according to scheme 2 and Eq. (13) is presented as a dotted line in the x, y plane. B, Schematic evaluation of B_{12} status. The data for a fictive patient (star) are interpreted as probability of coincidence with one or another frequency peak; see the main text for the details. C, Wellness parameter w as a linear function of B_{12} status expressed via logarithm of normalized holoTC·B_{12} (○, $R^2 = 0.82$) or MMA·Hcy (Δ, $R^2 = 0.80$).

(MMA·Hcy) on the surface x, y was analyzed (Fig. 5). The positive skewness introduced by multiplication of variables was compensated by square root and logarithmic transformations [30,31]. The data were fitted by a sum of bivariate Gaussian functions [29]:

$$z_{(x,y)} = \sum z_{i(x,y)} = \sum Z_i \cdot e^{-\frac{1}{2}\left\{\frac{(x_i-\mu_{i,x})^2}{\sigma_{i,x}^2} + \frac{(y_i-\mu_{i,y})^2}{\sigma_{i,y}^2}\right\}} \qquad (12)$$

where each individual function $z_{i(x,y)}$ describes a peak of frequency Z_i with maximum at $x = \mu_{i,x}$, $y = \mu_{i,y}$ and the standard deviations $\sigma_{i,x}$, $\sigma_{i,y}$ directed along the corresponding axes. Eq. (12) ignores correlation between x and y, which is sufficiently accurate within a local area of the x,y surface and/or at $-0.3 < R < 0.3$.

2.3.6. Dynamics of metabolic response

In the previous sections, concentrations of plasma B_{12}, MMA, and Hcy were related to holoTC using the fitting functions in Figs. 2A and 3A. This connection stipulates the relative changes of all components in response to altered B_{12} intake, which increases holoTC by 1% ($TC_{+1\%} = 1.01 \cdot TC_0$). The concentrations and relative sensitivities $(S - S_0)/S_0 \cdot 100\%$ of metabolites (S = B_{12}, MMA, or Hcy) were calculated within a wide interval of holoTC, and the simulated curves were plotted as functions of $(\text{holoTC} \cdot B_{12})^{1/2}$ (Fig. 7A). The marker with the highest response (in absolute units) is the most sensitive indicator of B_{12} absorption.

Another aspect of dynamic changes concerns the global metabolic response to B_{12} intake. Differentiation of Eq. (10) gives an estimate of such effect:

$$\frac{dy}{dx} = -\frac{P_2 \cdot P_3 \cdot x}{(P_3 + x)^2} \qquad (13)$$

The value of dy/dx (the response coefficient) quantitatively describes the dynamics of Cbl-dependent metabolic network when moving from one steady state to another (see "Results" and "Discussion" for more details).

3. Results

3.1. Dependence of total plasma B_{12} on holoTC

Three populations (Hlt, Sus, and *Veg*; "Methods") were analyzed as one set of points covering gradual transition between B_{12}-saturated and B_{12}-depleted metabolic states (Fig. 2A). Each individual was depicted as a point according to his/her marker values. Dependence of total B_{12} on holoTC was adequately fitted by Eq. (5) derived in accordance with scheme 1 (Fig. 1). Parameters of the best approximation ($\mu \pm$ SE) were as follows: $V_{d1} = 207 \pm 26$ pmol/L (total plasma B_{12} proportional to the maximal efflux from depot 1); K_{d1} =

12 ± 4 pmol/L (concentration of plasma holoTC that guarantees half-maximal efflux of holoHC from depot 1); K_{34} = 0.88 ± 0.16 (a constant related to equilibrium $M_1 \leftrightarrow M_2$ via depot 2 and excretion).

The global fit in Fig. 2A deviated from the experimental results at low holoTC, where points from populations Sus and Veg were situated above and below the tendency curve, respectively. Therefore, the 2 data sets were analyzed separately (Fig. 2B, holoTC <50 pmol/L) using the equation of transitional kinetics (Eq. [6] with floating zero). The linear coefficient (K_{34} + 1) was assigned to 1.9 in accordance with the fit from Fig. 2A. The following parameters of best approximation (μ ± SE) were obtained: Sus V_{d1} = 201 ± 32 pmol/L, K_{d1} = 5.6 ± 9 pmol/L, and δM = 3.5 ± 16 pmol/L (Fig. 2B, dash-dotted line); and Veg V_{d1} = 106 ± 32 pmol/L, K_{d1} = 14 ± 21 pmol/L, and δM = −7.7 ± 5.8 pmol/L (Fig. 2B, long dashes). The population Sus had high V_{d1} and positive δM, which corresponded to the saturated depot 1. Vegans were characterized by low V_{d1} and negative δM, which were interpreted as the depleted depot 1 (see "Discussion" for the details).

3.2. Dependence of plasma MMA and Hcy on holoTC and B_{12}

Fig. 3 shows logarithmic concentrations of plasma Hcy, MMA, or their geometric mean presented as functions of plasma holoTC, total B_{12}, or $(holoTC \cdot B_{12})^{1/2}$. The theoretical background of the chosen coordinate systems is described in "Methods." Fittings by Eq. (8) (Fig. 3A, B, C) and Eq. (10) (Fig. 3D) are shown as thick solid lines, and the parameters of best approximation are presented in Table 1. Comparison of 4 different 2-dimensional (2D) coordinate systems demonstrates that averaging of variables (Fig. 3D) essentially improves goodness of fit (compare R^2 in Table 1). Altogether, the suggested model described the data much better than the linear function (eg, MMA vs holoTC, R^2 = 0.054, not shown).

The parameters of best approximation P_i (Table 1) and Eqs. (9a), (9b), and (9c) were used for complete description of the metabolic system under a few additional assumptions. Thus, the influx v_{1s} was set to 1. The half-saturation coefficients of S excretion (K_2) and Cbl-dependent conversion (K_3) were equated to $5 \cdot S_{normal}$ and S_{normal}, respectively (see subscript to Table 2). These assumptions are based on the idea that catalytic conversion of MMA and Hcy via v_{3s} prevails under the normal conditions, whereas increase in metabolite concentrations accelerates excretion via v_{2s} [27,28]. The shown K_i values satisfy the requirement of S/K_2 and S/K_3 greater than 0.1; that is, all LinLog fluxes are positive. Finally, the values of V_{2s} (maximal excretion), V_{3s} (maximal velocity of Cbl reaction), and K_X (half-saturation with the extracellular Cbl) were estimated (Table 2) and used in the analysis below of disturbing effects, irrelevant to Cbl.

Thus, evaluation of B_{12} status solely by MMA or Hcy is weakened by the objective source of error—existence of Cbl-independent fluxes v_{1s} and v_{2s}. Scheme 2 helps to simulate the response of S to their change (Fig. 3, thin lines). All charts demonstrate that manipulations with the S influx (v_{1s}) significantly shift the tendency curve either upward ($1.5 \cdot v_{1s}$) or downward ($0.5 \cdot v_{1s}$). The region in between includes most of the experimental points. Comparison of panels in Fig. 3 clearly displays decreased dispersion of points in the averaging coordinates (Fig. 3D), where only a few results fall outside the boundaries $1.5 \cdot v_{1s}$ and $0.5 \cdot v_{1s}$. Simulation of the changed S excretion ($2 \cdot V_{2s}$ or $0.4 \cdot V_{2s}$) shows its low impact on the system (Fig. 3) especially at high concentrations of holoTC and B_{12}. The above analysis means that the major source of error is variation of the production velocity (v_{1s}) but not the excretion velocity (v_{2s}). The latter process is potentially related to renal function. For example, a decreased value of v_{2s} might correspond to renal dysfunction (if this syndrome is confined to kidney but does not reflect some general metabolic disorder). This subject deserves a separate investigation, which is beyond the scope of current publication.

The presented model adequately described biochemical transition between the normal and B_{12}-deficient metabolism. Statistical analysis of the data was then undertaken to find the most frequent combinations of the markers corresponding to different stages of Cbl-depletion.

Table 2
Parameters of the metabolic networks described by scheme 2

Dependency	V_2	V_3	K_X (pmol/L)
Fig. 3A log(MMA) vs holoTC	1.17	2.31	35
Fig. 3A log(Hcy) vs holoTC	1.48	2.06	19
Fig. 3B log(MMA) vs B_{12}	1.72	2.59	327
Fig. 3B log(Hcy) vs B_{12}	2.35	1.96	151
Fig. 3C log(MMA) vs $(holoTC \cdot B_{12})^{1/2}$	1.16	2.62	104
Fig. 3C log(Hcy) vs $(holoTC \cdot B_{12})^{1/2}$	1.08	2.26	44
Fig. 3D ½log(MMA·Hcy) vs $(holoTC \cdot B_{12})^{1/2}$	1.17[a]	2.40[b]	70

The values were calculated assuming v_{1s} = 1; $\log_{10}(K_2)$ = 0 and $\log_{10}(K_3)$ = −0.7 for MMA; and $\log_{10}(K_2)$ = 1.7 and $\log_{10}(K_3)$ = 1 for Hcy.

[a] Mean value of $\log_{10}(K_2)$ for MMA and Hcy was used to calculate the apparent V_2.

[b] Mean value of $\log_{10}(K_3)$ for MMA and Hcy was used to calculate the apparent V_3.

3.3. Distributions of holoTC, B_{12}, MMA, Hcy, and analysis of reference groups

The monovariate probability distributions of 4 markers in preselected Hlt, Sus, and Veg populations [14,17,22] were depicted as frequency polygons (Fig. 4). The obtained distribution patterns pointed to a nonhomogeneous composition of the populations. The data were approximated by a sum of Gaussian functions (Eq. [11]), and the regression

fitting confirmed the presence of several frequency peaks. They corresponded to subgroups called *excellent* (*e*), *normal* (*n*), *transitional* (*t*), and *deficient* (*d*) (see tags in Fig. 4). This classification suits the approximate threshold limits presented in "Introduction," which separate the assumed healthy individuals ($n + e$) from the potentially deficient patients (d).

The subgroups had a dynamic nature revealed by oral administration of B_{12} to healthy individuals. Such treatment caused redistribution of frequency in favor of the *e* subgroup; see comparison of the population Hlt (before) and HltB (after B_{12} intake) in Fig. 4.

Monovariate distributions in Fig. 4 demonstrated noticeable overlaps of some peaks even in the preselected groups. Therefore, the pooled data set (Hlt + Sus + Veg) was analyzed in the averaging coordinates x, y (Fig. 5A), where dispersion of points is reduced. The 3-dimensional (3D) surface fitted by Eq. (12) revealed several major peaks: *e*, *n*, *t*, *d*, and *p* (position of *p* group is approximate because of its low representation). The peaks were assumed to be the metabolic fingerprints of different (sub)clinical groups (Table 3). The 2D ellipses in Fig. 4D graphically indicate the areas of $\mu_{i,xy} \pm \sigma_{i,x} \pm \sigma_{i,x}$ incorporating 68% of the representatives from each group. The shown boundaries were used to evaluate the characteristic concentrations of the markers associated with these subgroups (Table 3).

The detailed clinical description of the found subgroups was not undertaken because the earlier work conducted on the population Sus found "no association between the biochemical markers and symptoms possibly related to vitamin B_{12} deficiency" [22], although many participants responded biochemically to B_{12} treatment.

Fig. 5B shows a practical example of how B_{12} status should be assessed in x, y coordinates. Result for a fictive patient (star symbol) was placed on the x, y surface; and the distance to the neighboring peaks μ_t and μ_n was measured in σ units ($2.6\sigma_t$ and $0.8\sigma_n$, respectively). The corresponding tail areas under the standard Gaussian curve indicated 42% and 1% probability of equality with peaks *n* and *t*, respectively.

A less elaborate analysis of the data is also possible. Thus, the hyperbolic model (Fig. 3) subjected to LinLog transformation ("Mathematical justification of flux equations" in "Appendix A") predicts linear dependence of the data if working in full logarithmic coordinates. The chart in Fig. 5C uses this feature and introduces the wellness parameter w as a novel characteristic of Cbl-related metabolism: $w = \log_{10}(\text{holoTC}_n) + \log_{10}(B_{12n}) - \log_{10}(\text{MMA}_n) - \log_{10}(\text{Hcy}_n)$. This expression is based on the logarithmic presentation of the geometric mean of 4 normalized markers (eg, $\text{MMA}_n = \text{MMA}/\text{MMA}_{\text{normal}}$). Its value is strongly associated with the B_{12} status (Fig. 5C, $R^2 = 0.82$) expressed via pairwise combinations of the markers. Description of the subgroups by w coefficient is eye-catching (Fig. 5C, Table 3). For example, $w = 0 \pm 0.5$ indicates a nearly normal metabolism, whereas more negative values ($w < -1$) point to B_{12} deficiency.

3.4. Cutoff thresholds and receiver operating characteristic curves of the individual markers

The 4 independent metabolites have different ability to predict B_{12} deficiency. Therefore, they were examined separately using the wellness parameter w as the criterion standard, which sorted all individuals into the groups assumed deficient ($w \le -0.516$) and assumed healthy ($w > -0.516$). The obtained distributions (Fig. 6A) revealed the optimal cutoff values (Fig. 6A, vertical lines) for the individual markers. According to the performed analysis, a patient should be considered as B_{12} deficient (Fig. 6A, dark area) at holoTC less than or equal to 36 pmol/L, total B_{12} less than or equal to 207 pmol/L, MMA greater than or equal to 0.38 μmol/L, and Hcy greater than or equal to 14.7 μmol/L if diagnosis is based on a single marker. Reliability of such prediction decreases in the range holoTC, MMA, B_{12}, and Hcy, as follows from the area under curve values of receiver operating characteristic (ROC) curves (Fig. 6B). Two most reliable markers (holoTC and MMA) are suitable for determination of B_{12} status using a shortened variant of

Table 3
Metabolic characteristics (mean ± SD) of the subgroups found within the pooled population Hlt + Sus + Veg (Figs. 3A and 5A)

Marker	Pernicious? (*p*)	Subgroups and their metabolic parameters			
		Deficient (*d*)	Transitional (*t*)	Normal (*n*)	Excellent (*e*)
$x = (\text{holoTC}\cdot B_{12})^{1/2}$ (pmol/L)	16 ± 8	43 ± 13	78 ± 13	107 ± 15	142 ± 42
$y = \frac{1}{2}\log(\text{MMA}\cdot\text{Hcy})$ $\log_{10}(\mu\text{mol/L})$	1.2 ± 0.16	0.60 ± 0.19	0.37 ± 0.15	0.25 ± 0.10	0.15 ± 0.16
holoTC (pmol/L)	12.5[b]	19.4	31.2	48.1	65.7
Total B_{12} (pmol/L)	20.6	95.5[c]	195[d]	238	307
MMA (μmol/L)	3.06	0.84	0.405	0.287	0.219
Total Hcy (μmol/L)	82.1	18.9	13.6	11.0	9.11
w[a] $= \log_{10}(\text{hTC}_n\cdot\text{B12}_n) - \log_{10}(\text{MMA}_n\cdot\text{Hcy}_n)$	−2.55	−1.49	−0.516	0.0	0.445
$w_{T/M}$[a] $= \log_{10}(\text{hTC}_n) - \log_{10}(\text{MMA}_n)$	−1.54	−0.861	−0.338	0.0	0.253

[b, c, d] The values are very close to (b) half-saturation parameter K_{d1} of depot 1 in the mixed population ("Dependence of total plasma B_{12} on holoTC," Fig. 2A) and concentration of total B_{12} maintained exclusively by depot 1 (V_{d1}) in (c) population Veg ("Dependence of total plasma B_{12} on holoTC," Fig. 2B) and (d) mixed group ("Dependence of total plasma B_{12} on holoTC," Fig. 2A).

[a] Wellness (w) and $w_{T/M}$ parameters were calculated using the concentrations of metabolites normalized by division by the corresponding normal concentrations; for example, $\text{MMA}_n = \text{MMA}/\text{MMA}_{\text{normal}}$.

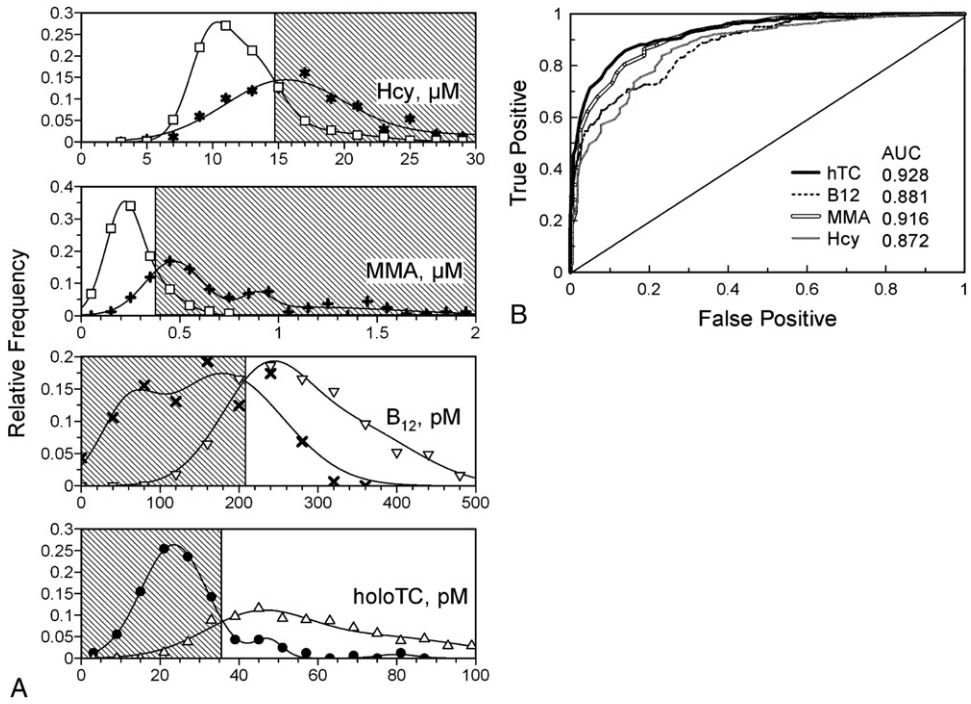

Fig. 6. Cutoff thresholds and ROC analysis of 4 separate markers. A, Relative frequencies of the groups assumed deficient ($w \leq 0.516$, closed symbols) and assumed healthy ($w > 0.516$, open symbols) plotted vs concentrations of the metabolic markers. Vertical lines indicate the optimal cutoff thresholds. Dark areas show deficient (positive) cases according to the cutoff limits. B, Receiver operating characteristic curves of the 4 markers, where the wellness parameter $w = 0.516$ was used as a separator of the groups assumed deficient and assumed healthy.

wellness parameter $w_{T/M} = \log_{10}(\text{holoTC}_n) - \log_{10}(\text{MMA}_n)$ (Table 3) if measurements of all 4 markers are difficult.

3.5. Dynamics of metabolic response

If the steady-state analysis cannot provide a clear-cut result, the dynamic approach appears to be a valuable tool of refined diagnostics.

3.5.1. Simulation of metabolic responses to B_{12} administration

Interdependence between 4 markers (Eqs. [5] and [8], and Figs. 2A and 3A) helped to simulate their sensitivities to absorption of B_{12}. Assuming that the intake of B_{12} causes an increase in holoTC by 1%, the corresponding responses of other metabolites were calculated ("Methods"). The produced curves (Fig. 7A) indicated that the sensitivities depended on the initial B_{12} status. Thus, the best sensors of B_{12} uptake for the transitional metabolism were holoTC and MMA; but under extreme vitamin saturation, B_{12} showed a better performance than MMA.

The global metabolic response was simulated by differentiation of the steady-state approximation function (Fig. 3D) that strictly stipulates the effect of changing B_{12} on concentrations of the enzyme substrates. In other words, the shape of the steady-state curve (expressed as dy/dx) is treated as a B_{12}-dependent variable. The produced differential curves (Fig. 7B) were obtained using Eq. (13) and the fitting parameters from Table 1 (data for Fig. 3D). Whereas the

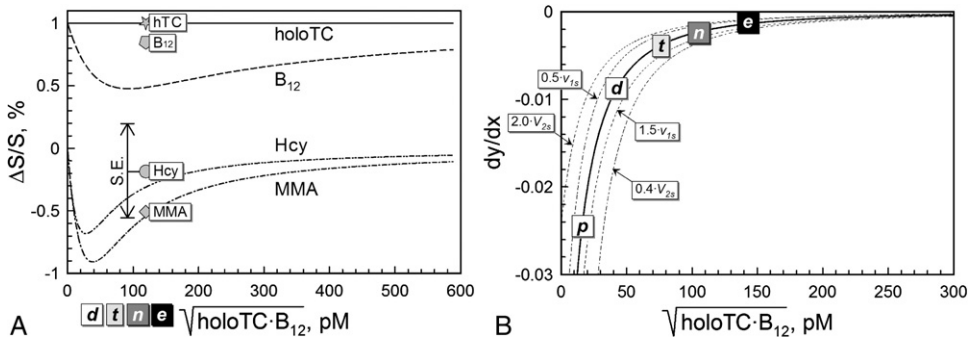

Fig. 7. Simulation of the metabolic response. A, Relative sensitivities of the markers toward changing B_{12} intake (curves). Gray symbols indicate the means of experimental measurements [14]. Dispersion of $\Delta S/S$ for Hcy ($\mu \pm$ SE) is shown as a typical example of the experimental error. B, Global metabolic response simulated for the main model (thick line) and the changed fluxes v_{1s} and v_{2s} (thin lines).

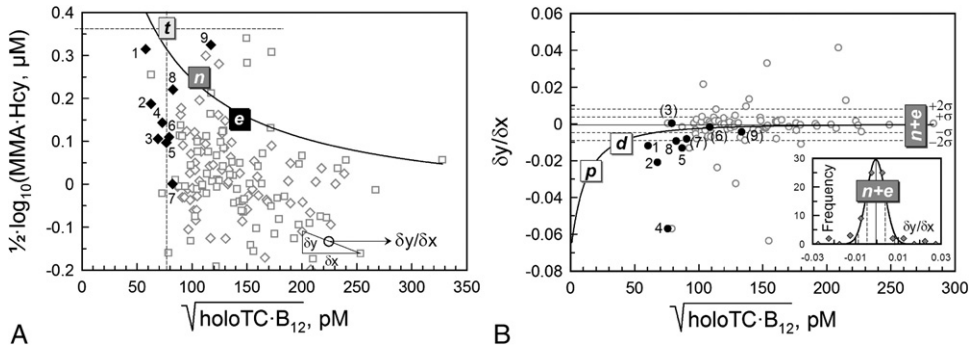

Fig. 8. Analysis of the global metabolic response in the population Hlt. A, Markers of B_{12} deficiency at steady state presented in the averaging coordinates: day 1 (before B_{12} treatment, ◊) and day 8 (after B_{12} treatment, □). Calculation of a derivative $\delta y/\delta x$ (○) for one individual is illustrated by the triangle. The general tendency curve of the pooled population (Hlt + Sus + Veg) is presented as a thick line. Filled diamonds notate 9 ambiguous cases. B, Analysis of the derivative $\delta y/\delta x$. Ambiguous measurements from Fig. 8A are indicated by filled circles. Numbers with and without brackets notate ambiguous cases considered as healthy and deficient, respectively. Inset presents the probability distribution of $\delta y/\delta x$ fitted by Eq. (11).

essential dynamic changes ($dy/dx \le -0.01$) characterized B_{12}-deficient condition, the response of normal and excellent groups was sufficiently close to zero ($dy/dx > -0.003$) (see thick solid line in Fig. 7B). Behavior of the derivative dy/dx was affected by Cbl-independent fluxes (thin lines with tags). In contrast to coordinates y vs x (Fig. 3D), the effect of v_{1s} on the differential function was moderate (Fig. 7B); and the major source of disturbance was the flux v_{2s}. In other words, presentation of data in the steady-state and differential coordinates suppresses fluctuations of different Cbl-independent fluxes.

3.5.2. Analysis of the experimental results

Hvas et al [14], working with Hlt individuals, described the effect of B_{12} administration on the plasma holoTC, B_{12}, MMA, and Hcy. The concentrations measured at first visit were notated as day 1 and, after receiving B_{12}, as day 8 (see "Methods" for details). The relative sensitivities were calculated $S_{\%} = (S_{day8} - S_{day1})/S_{day1}\cdot 100\%$ and related to holoTC (eg, $S_{\%MMA}/S_{\%holoTC}$). The mean results are shown in Fig. 7A (gray symbols). They correlated with the simulated curves, although high dispersion of the experimental data (eg, $\mu \pm$ SE for Hcy in Fig. 7A) precluded accurate interpretation.

Global metabolic response to B_{12} treatment (ie, transition from day 1 to day 8) is analyzed in Fig. 8A. Derivatives $\delta y/\delta x$ were calculated for each individual (see triangle in Fig. 8A), and the obtained results are shown in Fig. 8B. Both Fig. 8A and Fig. 8B contain also the tendency curves (thick lines) from previous fittings in Figs. 3D and 6B, respectively. Most of the measurements at day 1 (A, open diamonds) were classified as "normal" or "excellent." However, 9 individuals (Fig. 8A, filled diamonds) appeared in the transitional region. Two of them had also relatively low wellness coefficients (№ 1, $w = -0.66$; № 2, $w = -0.34$). All 9 responses (Fig. 8B, filled circles) were compared with the Gaussian distribution of $\delta y/\delta x$ (Fig. 8B, inset); and the individuals № 3, 6, 7, and 9 were classified as "normal," whereas № 1, 2, 4, 5, and 8 seemed to be deficient because their responses were below the 95% confidence limits of $n + e$ group (see "Discussion." for details).

4. Discussion

The main purpose of the present investigation is to make diagnostics of B_{12}-related disorders unambiguous despite at times contradictory indications from 4 independent tests. Therefore, the commonly accepted metabolic markers of B_{12} deficiency, measured in a broad population sample, were assembled in one working field and subjected to kinetic and statistic analysis. The results are discussed in terms of the metabolic effect, laying the foundation for a novel diagnostic approach.

4.1. Metabolic connection of plasma B_{12} and holoTC

Dependency of the total plasma B_{12} on concentration of holoTC (Fig. 2A) was analyzed in the joint group (Hlt + Sus + Veg). The fitting model is shown in scheme 1 (Fig. 1), where 2 storage compartments (depot 1 and depot 2) mediate exchange of Cbl between the pools of TC and HC. Depot 1 seems to be a specific depository (possibly related to liver) saturated with Cbl at low concentration of holoTC. At maximal saturation, this storage provides an efflux capable to maintain approximately 200 pmol/L steady-state concentration of holoHC in blood plasma. This value coincides with B_{12} in the transitional subgroup (Table 3), where depot 1 still supplies the necessary vitamin minimum. The other storage (depot 2) is regarded as an unspecific surplus depository, possibly present in different tissues. It accumulates Cbl at high concentration of the vitamin in blood and maintains the ratio holoHC/holoTC ≈ 1.

Scheme 1 describes an ideal steady state, where occasional fluctuations of holoTC are ignored. Yet, they seem to play an essential role under experimental measurements, where a deviation of total B_{12} from zero was found at holoTC → 0 (Fig. 2B). The obtained results were interpreted as the ability of depot 1 to "buffer" total plasma B_{12}. Thus,

Sus individuals seemed to have a relatively saturated depot 1, able to maintain total B_{12} at the level of ≈100 pmol/L despite a sudden fall of holoTC to less than 5 pmol/L (Fig. 2B, dash-dotted line). On the contrary, the group Veg had depleted depot 1, which absorbed up to 8 pmol/L of plasma holoTC without any efflux of Cbl (Fig. 2B, long dashes). An essential delay in the response of total B_{12} to the fast-changing holoTC concentration causes occasional contradictions between these markers, as discussed by Herbert et al [18] in an early work. The reason for plasma holoTC fluctuations is unknown, but changed uptake and/or regulated secretion to blood might be the explanations.

4.2. MMA and Hcy as functions of B_{12} and holoTC

A steady-state network (scheme 2, Fig. 1) approximated the dependence of MMA and Hcy on plasma Cbl in the pooled data set Hlt + Sus + Veg (Fig. 3). Behavior of the model was tested under different conditions. It was found that the Cbl-dependent utilization of S (flux v_{3s}) was not the only metabolic branch affecting the steady-state concentrations of MMA or Hcy (S). Thus, small changes in the production velocity (v_{1s}) caused noticeable shifts (Fig. 3, thin curves with v_{1s} tags), whereas the effect of excretion velocity (v_{2s}) was conditional (Fig. 3, thin curves with V_{2s} tags). In other words, changes of v_{2s} and especially v_{1s}, although irrelevant in terms of Cbl-metabolism, present a hindrance for correct evaluation of B_{12} status if based exclusively on measurements of either MMA or Hcy.

4.3. Compensation of errors

The performed analysis revealed 3 major sources of errors negatively affecting diagnostics of B_{12} deficiency: (1) transitional fluctuations of holoTC, (2) delayed response of total B_{12} to these fluctuations, and (3) variations in the Cbl-independent production and excretion fluxes of MMA and Hcy. The expected random character of these disturbances allows, however, their partial compensation by pairwise averaging of the variables according to Eqs. (A7), (A8) ("Appendix A"), and (10) ("Methods"). After the suggested transformation of coordinates (Fig. 3D), the coefficient of determination (R^2 in Table 1) essentially increased because of lower dispersion of points around the tendency curve. This would facilitate detection of the reference subgroups characterized by frequent combinations of the markers. Therefore a comparative analysis of probability distributions was conducted in 2D/3D coordinates.

4.4. Probability distributions of subgroups and assessment of B_{12} deficiency

On the first step, the markers of B_{12} deficiency were analyzed independently as the standard monovariate distributions (Fig. 4). Fitting of the separate data sets Hlt, Sus, and Veg by a sum of Gaussian functions exposed several frequency peaks present within each population (Fig. 4). The corresponding subgroups were not associated with age, sex, or any other eye-catching feature and, therefore, were ascribed to difference in B_{12} status. In most cases, the frequency peaks significantly differed from the means and medians of populations.

To avoid overlaps of the distribution peaks, visible in 2D coordinates (Fig. 4), bivariate analysis was performed in the averaging 3D coordinates to reach a better resolution (Fig. 5A). This approach revealed e, n, t, d, and p peaks even working with the pooled data set (Hlt + Sus + Veg). Existence of several clusters may be interpreted in terms of stable and unstable physiologic states, where peaks of frequency represent the metabolic fingerprints of stable metabolic systems.

Association of a patient with a metabolic group can be estimated by either the distance between his/her marker point and the nearest maximum (Fig. 5B) or the value of wellness parameter w (Fig. 5C, Table 3). The latter coefficient includes all 4 markers and is convenient for interpretation. Thus, positive or slightly negative values indicate normal metabolism, whereas more negative values suggest B_{12} deficiency; for example, $w = -0.5$ for transitional and -1.5 for deficient groups. One unifying variable also simplifies computer-based sorting of the data during automated analysis of large populations.

Detailed clinical characterization of each detected subgroup was hardly possible because clinical symptoms are diffuse unless a severe B_{12} deficiency is developed [6,9,22]. Yet, the metabolic groups e, n, t, and d were compared in terms of hemoglobin concentration taken as a marker of anemia (data from Hvas and Nexø [22]). The 68% representative regions (ellipses in Fig. 3D) were used to select the samples. Comparison of the hemoglobin data by the nonparametric Kolmogorov-Smirnov test revealed a very low probability ($P < .01$) of equal distribution for the pairs $d \neq n$, $d \neq e$, $t \neq n$, and $t \neq e$, whereas the pairs $d = t$ and $n = e$ were likely to be equal ($P \approx .7$). The deficient group (d) had low hemoglobin monomer concentration ($\mu \pm SE = 8.13 \pm 0.20$ mmol/L, n = 15) approaching anemia (<8 mmol/L), whereas the "normal" individuals (8.73 ± 0.05 mmol/L, n = 97) were well within the normal boundaries (8-10 mmol/L).

4.5. Reliability of separate markers and simplified assessment of B_{12} deficiency

The complete metabolic analysis involving all 4 markers is not always convenient from the practical point of view. Therefore, the predictive potential of separate markers was examined in terms of their cutoff thresholds and ROC curves (Fig. 6) using the wellness parameter w as the criterion standard ("Cutoff thresholds and receiver operating characteristic curves of the individual markers"). The obtained cutoff limits of holoTC, MMA, and Hcy (Fig. 6A) were close to those reached by general assent ("Introduction"). Only the threshold of B_{12} from the present analysis (207 pmol/L) deviated from the commonly used value of 150 pmol/L. The latter is historically based on clinical indications and

probably reflects a higher degree of deficiency than that of the transitional metabolic state. Reliability of the individual markers decreases in the order holoTC, MMA, total B_{12}, and Hcy, according to the produced ROC curves (Fig. 6B). Good characteristics of holoTC and/or MMA are often mentioned in the literature [9,12,13,20,22], and holoTC/MMA-based coefficient $w_{T/M}$ (shortened wellness parameter, Table 3) may provide a substitute for the full-scale test.

4.6. Analysis of metabolic response

Determination of the steady-state concentration of a metabolite is a well-known method to characterize the related biochemical or physiologic processes. At the same time, application of the dynamic metabolic perturbations as a diagnostic tool is relatively rare. The section below discusses details of this approach in terms of sensitivity of the individual markers and their global response to B_{12} uptake.

The markers of B_{12} deficiency have different sensitivities to altered intake of the vitamin. Naturally, the B_{12} absorption test performs better with the most responsive reporter. The experimental attempts to detect such reporter were unfortunately compromised by high dispersion of the results [14]. Therefore, the theoretical estimation, based on a much larger database of the steady-state measurements, was carried out in the present publication. The performed modeling (Fig. 7A) demonstrates that holoTC is the most sensitive indicator of B_{12} absorption throughout the whole scale. Relative changes of other markers (B_{12}, MMA, Hcy) are dependent on the initial B_{12} status and do not give the ultimate answer.

The fact that metabolic changes of the markers correlate with the initial B_{12} status may be particularly useful in diagnostics of B_{12} deficiency, especially in doubtful cases [9]. Intuitively, a small dose of B_{12} given to a Cbl-deficient patient would cause a significant perturbation, whereas a healthy person would not respond at all. Differentiation of the combined steady-state function $y_{(x)}$ from Fig. 3D expresses these deductions in the exact units of global response: $dy/dx \approx -0.002$ at normal B_{12} and $dy/dx < -0.01$ under deficiency (Fig. 7B). In addition, differentiation is advantageous in another aspect. Most outliers of the steady-state measurements originate from the changing influx v_{1s}, which shifts the tendency curve either upward or downward (Fig. 3), generally maintaining its shape. Differential function dy/dx is insensitive to such transposition (see modeling in Fig. 7B), and the response to B_{12} treatment would disclose the true B_{12} status of a patient with abnormal v_{1s} unless the excretion efflux (v_{2s}) is also altered. The latter case makes interpretation nearly impossible.

Practical approach to evaluation of the global metabolic response is presented in Fig. 8. For each individual, the initial metabolic point (day 1, diamond) was related to the value after administration of B_{12} (day 8, square) by calculating the response coefficient $\delta y/\delta x$. Judged from the day 1 measurements, the majority of participants had either "normal" or "excellent" metabolism (Fig. 8A). Yet, 9 individuals (Fig. 8A, filled diamonds) had contradictory indications of x and y (eg, transitional x and excellent y). The ambiguous data were tested by differentiation, and 56% of the results indicated B_{12} deficiency by falling below the lower confidence limit of $n + e$ distribution (Fig. 8B; filled circles 1, 2, 4, 5, and 8). Such response is abnormal because only 9% of the "normal" points (Fig. 8B, open circles) fell below the limit of $\mu - 2\sigma$. The presented differential method appears to be a promising tool of diagnostics, although a broader experimental data set is required to improve the accuracy.

4.7. Conclusions

The designed model of B_{12} turnover in plasma was validated by good approximation of the experimental data. Manipulations with the model revealed the major sources of error affecting assessment of the vitamin status and suggested a way of their compensation. Finally, 4 markers of B_{12} deficiency were mathematically connected and presented in one coordinate system, where dispersion of points was decreased. The produced probability surface exposed several frequent marker combinations suggested as the references values for different types of B_{12} metabolism. The concept of wellness parameter was introduced to treat all the markers as a single variable, simplifying classification of the data. The dynamic metabolic response to B_{12} administration was mathematically described as an additional method of diagnostics when classifying ambiguous cases.

Acknowledgment

I would like to express my sincere gratitude to E Nexø, ZL Wright, AM Hvas, J Møller, TAB Sanders, and AL Mørkbak for the original data sheets containing plasma concentrations of the markers of B_{12} deficiency. Discussions with Prof E Nexø, Dr N Fedosova, and Dr A McCaddon were extremely valuable for the presentation of the material. The work was supported by Cobento.

Appendix A. *Mathematical justification of flux equations*

Eqs. (1), (2), and (3) were used to approximate an arbitrary metabolic flux. The origin of hyperbolic function is sufficiently transparent [23,32]; and in most cases, Eq. (1) fits the whole range of a quasi-hyperbolic process. The linear expression (Eq. [2]) approximates the initial part of a quasi-hyperbolic saturation curve ($v \le 0.4 \cdot V$) and becomes even preferable if the dependence is quasi-linear [23], slope $\approx V/(1.1 \cdot K)$. The mathematical nature of LinLog approximation (Eq. [3]) has never been elucidated and requires an explanation. It is based on a shortened logarithmic expansion:

$$log_e(x) = 2\frac{(x-1)}{(x+1)} + \frac{2}{3}\frac{(x-1)^3}{(x+1)^3}\cdots \approx 2.3\frac{(x-1)}{(x+1)}$$
$$log_{10}(x) = \frac{(x-1)}{(x+1)} = \frac{2x}{(x+1)} - 1 \qquad \text{(A1)}$$

valid within the interval of $0.1 \le x \le 10$. The expression (A1) directly connects logarithmic and hyperbolic functions; and assuming $x = S/K$, one can easily obtainEq. [3] ("Methods"). For the sake of mathematical convenience, Eq. [3] was transformed to an alternative form:

$$v \approx a' + b' \cdot log_{10}(S) \tag{A2}$$

$$a' = \frac{V}{2} \cdot log_{10}\left(\frac{10}{K}\right);\ b' = \frac{V}{2}$$

where the empiric coefficients a' and b' are rendered in terms of quasi-Michaelis kinetics. Both a' and b' contain the component $V = k_{cat} \cdot E_0$, and they can be rewritten as $a' = a \cdot E_0$ and $b' = b \cdot E_0$.

Extended solution of scheme 2

The steady-state balance of scheme 2 was described with help of one influx, v_{1s} (a constant), and 2 effluxes, v_{2s} and v_{3s} (both LinLog dependent on S):

$$\begin{gathered} v_{1s} = v_{2s} + v_{3s} \\ v_{1s} = \{a_2' + b_2' \cdot log_{10}(S)\} + \{a_3' + b_3' \cdot log_{10}(S)\} \end{gathered} \tag{A3}$$

where $a_3' = a_3 \cdot E_{3C}$ and $b_3' = b_3 \cdot E_{3C}$ (E_{3C} is concentration of the active enzyme with bound Cbl). The steady-state Eq. (A3) was rearranged to express $\log_{10}(S)$ via E_{3C}:

$$log_{10}(S) = \frac{v_{1s} - a_2' - a_3 \cdot E_{3C}}{b_2' + b_3 \cdot E_{3C}} = \frac{\frac{Q}{b_3} - \frac{a_3}{b_3} \cdot E_{3C}}{\frac{b_2'}{b_3} + E_{3C}} \tag{A4}$$

where $Q = v_{1s} - a_2'$. The derived hyperbolic function was transformed to its typical form:

$$\begin{aligned} log_{10}(S) &= \frac{\frac{Q}{b_3} - \frac{a_3}{b_3} \cdot E_{3C} + \frac{Q}{b_2'} \cdot E_{3C} - \frac{Q}{b_2'} \cdot E_{3C}}{\frac{b_2'}{b_3} + E_{3C}} \\ &= \frac{Q}{b_2'} - \frac{\left(\frac{a_3}{b_3} - \frac{Q}{b_2'}\right)}{\frac{b_2'}{b_3} + E_{3C}} E_{3C} \end{aligned} \tag{A5}$$

Afterward, the Cbl-saturated fraction E_{3C} of the enzyme E_3 was expressed via a hyperbolic saturation function:

$$E_{3C} = \frac{E_3 \cdot \mathrm{Cbl_{intr}}}{K_{cbl} + \mathrm{Cbl_{intr}}} \tag{A6}$$

where $\mathrm{Cbl_{intr}}$ corresponds to either free or chaperon-bound intracellular cofactor that binds to the originally inactive enzyme. Expression of $\mathrm{Cbl_{intr}}$ via the extracellular pools of holoTC and total B_{12} is, however, required.

The intracellular Cbl depends on plasma holoTC, holoHC, and total B_{12} according to the equilibrium shown in scheme 3 (Fig. 1) and the ratios below:

$$\begin{gathered} \mathrm{Cbl_{intr}} = K_H \cdot \mathrm{holoHC};\ \mathrm{Cbl_{intr}} = K_T \cdot \mathrm{holoTC} \\ B_{12} = \mathrm{holoHC} + \mathrm{holoTC} = \left(\frac{1}{K_H} + \frac{1}{K_T}\right) \cdot \mathrm{Cbl_{intr}} = \frac{\mathrm{Cbl_{intr}}}{K_B} \end{gathered} \tag{A7}$$

where $1/K_B = 1/K_H + 1/K_T$. Other equilibriums (eg, holoHC ↔ holoTC ↔ $\mathrm{Cbl_{intr}}$) stipulate various combinations of K_H and K_T but do not change the general appearance of Eq. (A7). The produced equations demonstrate that both holoTC and total plasma B_{12} easily substitute for $\mathrm{Cbl_{intr}}$ in the saturation function Eq. (A6) with introduction of one additional equilibrium constant. Expression of $\mathrm{Cbl_{intr}}$ via geometric mean of holoTC and B_{12} is also possible:

$$\begin{gathered} \mathrm{Cbl_{intr}} = K_B \cdot B_{12};\ \mathrm{Cbl_{intr}} = K_T \cdot \mathrm{holoTC} \\ \mathrm{Cbl_{intr.}^2} = K_B \cdot K_T \cdot \mathrm{B_{12}} \cdot \mathrm{holoTC} \\ \mathrm{Cbl_{intr}} = \sqrt{K_B \cdot K_T} \cdot \sqrt{\mathrm{B_{12}} \cdot \mathrm{holoTC}} = K_{BT} \cdot \sqrt{\mathrm{B_{12}} \cdot \mathrm{holoTC}} \end{gathered} \tag{A8}$$

where $K_{BT} = (K_B \cdot K_T)^{1/2}$. The extracellular components substitute for $\mathrm{Cbl_{intr}}$ in Eq. (A6), giving a more general equation:

$$E_{3C} = \frac{E_3 \cdot X}{K_X + X} \tag{A9}$$

where E_{3C} is the Cbl-saturated enzyme; E_3 is the total concentration of the enzyme 3; X = holoTC, B_{12}, or $(B_{12} \cdot \mathrm{holoTC})^{1/2}$; and $K_X = K_{Cbl}/K_B$, K_{Cbl}/K_T, or K_{Cbl}/K_{BT}. Combination of Eqs. (A5) and (A9) gives after a few transformations the fitting equation (Eq. [8]) used to approximate the dependence of $\log_{10}(S)$ on X (see the main text).

References

[1] Allen HR. Human vitamin B12 transport proteins. Prog Hematol 1975;9:57-84.

[2] Fedosov SN. Physiological and molecular aspects of cobalamin transport. In: Stanger O, editor. Water-soluble vitamins: subcellular biochemistry. Vienna: Springer; 2010. [in press].

3] Moestrup SK, Verroust PJ. Megalin- and cubilin-mediated endocytosis of protein-bound vitamins, lipids, and hormones in polarized epithelia. Annu Rev Nutr 2001;21:407-28.

[4] Nexø E. Cobalamin binding proteins. In: Kräutler B, Arigoni D, Golding BT, editors. Vitamin B_{12} and B_{12}-proteins. Weinheim: Wiley-VCH; 1998. p. 461-75.

[5] Bor MV, Nexø E, Hvas AM. Holo-transcobalamin concentration and transcobalamin saturation reflect recent vitamin B_{12} absorption better than does serum vitamin B_{12}. Clin Chem 2004;50:1043-9.

[6] Elin RJ, Winter WE. Methylmalonic acid: a test whose time has come? Arch Pathol Lab Med 2001;125:824-7.

[7] Scott JM. Folate and vitamin B_{12}. Proc Nutr Soc 1999;58:441-8.

[8] Baik HV, Russell RM. Vitamin B_{12} deficiency in the elderly. Annu Rev Nutr 1999;19:357-77.

[9] Carmel R, Green R, Rosenblatt S, et al. Update on cobalamin, folate, and homocysteine. Hematology Am Soc Hematol Educ Program 2003;2003:62-81.

[10] Jacobsen DW, Catanescu O, Dibello PM, et al. Molecular targeting by homocysteine: a mechanism for vascular pathogenesis. Clin Chem Lab Med 2005;43:1076-83.

[11] Chen X, Remacha AF, Sarda MP, et al. Influence of cobalamin deficiency compared with that of cobalamin absorption on serum holo-transcobalamin II. Am J Clin Nutr 2005;81:110-4.

[12] Goringe A, Ellis R, McDowell I, et al. The limited value of methylmalonic acid, homocysteine and holotranscobalamin in the diagnosis of early B_{12} deficiency. Haematologica 2006;91:231-4.

[13] Herrmann W, Obeid R, Schorr H, et al. The usefulness of holotranscobalamin in predicting vitamin B_{12} status in different clinical setting. Curr Drug Metab 2005;6:47-53.
[14] Hvas AM, Mørkbak AL, Nexø E. Plasma holotranscobalamin compared with plasma cobalamins for assessment of vitamin B_{12} absorption; optimisation of a non-radioactive vitamin B_{12} absorption test (CobaSorb). Clin Chim Acta 2007;376:150-4.
[15] Loikas S, Lopponen M, Suominen P, et al. RIA for serum holotranscobalamin: method evaluation in the clinical laboratory and reference interval. Clin Chem 2003;49:455-62.
[16] Miller JW, Garrod MG, Rockwood AL, et al. Measurement of total vitamin B_{12} and holotranscobalamin, singly and in combination, in screening for metabolic vitamin B_{12} deficiency. Clin Chem 2006;52: 278-85.
[17] Wright ZL, Hvas AM, Møller J, et al. Holotranscobalamin as an indicator of dietary vitamin B_{12} deficiency. Clin Chem 2003;49:2076-8.
[18] Herbert V, Fong W, Gulle V, et al. Low holotranscobalamin II is the earliest serum marker for subnormal vitamin B_{12} (cobalamin) absorption in patients with AIDS. Am J Hematol 1990;34:132-9.
[19] Nexø E, Christensen AL, Hvas AM, et al. Quantification of holotranscobalamin, a marker of vitamin B_{12} deficiency. Clin Chem 2002;48:561-2.
[20] Nexø E, Hvas AM, Øyvind B, et al. Holo-transcobalamin is an early marker of changes in cobalamin homeostasis. A randomized placebo-controlled study. Clin Chem 2002;48:1768-71.
[21] Ulleland M, Eilertsen I, Quadros EV, et al. Direct assay for cobalamin bound to transcobalamin (holo-transcobalamin) in serum. Clin Chem 2002;48:526-32.
[22] Hvas AM, Nexø E. Holotranscobalamin—a first choice assay for diagnosing early vitamin B_{12} deficiency? J Intern Med 2005;257: 289-98.
[23] Legent G, Thellier M, Norris V, et al. Steady-state kinetic behaviour of two- or n-enzyme systems made of free sequential enzymes involved in a metabolic pathway. C R Biologies 2006; 329:963-6.
[24] Wu L, Wang W, van Winden WA, et al. A new framework for the estimation of control parameters in metabolic pathways using lin-log kinetics. Eur J Biochem 2004;271:3348-59.
[25] Fedosov SN, Berglund L, Fedosova NU, et al. Comparative analysis of cobalamin binding kinetics and ligand protection for intrinsic factor, transcobalamin and haptocorrin. J Biol Chem 2002; 274:26015-20.
[26] Fedosov SN, Fedosova NU, Kräutler B, et al. Mechanisms of discrimination between cobalamins and their natural analogues during their binding to the specific B_{12}-transporting proteins. Biochemistry 2007;46:6446-58.
[27] Guttormsen AB, Schneede J, Ueland PM, et al. Kinetics of total plasma homocysteine in subjects with hyperhomocysteinemia due to folate or cobalamin deficiency. Am J Clin Nutr 1996;63: 194-202.
[28] Kwok T, Cheng G, Lai WK, et al. Use of fasting urinary methylmalonic acid to screen for metabolic vitamin B_{12} deficiency in older persons. Nutrition 2004;20:764-8.
[29] Abramowitz M, Stegun IA. Handbook of mathematical functions with formulas, graphs, and mathematical tables. 9th ed. New York: Dover Publications; 1972.
[30] Kirkwood BR, Sterne AC. Essential medical statistics. 2nd ed. Oxford: Blackwell Science; 2003.
[31] Limpert E, Stahel W, Abbt M. Log-normal distributions across the sciences: keys and clues. BioScience 2001;51:341-52.
[32] Cornish-Bowden E. Fundamentals of enzyme kinetics. 3rd ed. London: Portland Press; 2004.